frontiers | Frontiers in Earth Science

TYPE Original Research
PUBLISHED 27 December 2023
DOI 10.3389/feart.2023.1280787

OPEN ACCESS

EDITED BY
Hu Wang,
Southwest Jiaotong University, China

REVIEWED BY
Yanbao Li,
China Earthquake Administration, China
An Li,
China Earthquake Administration, China

*CORRESPONDENCE
Xi Li,
lixgj@126.com

RECEIVED 21 August 2023
ACCEPTED 08 November 2023
PUBLISHED 27 December 2023

CITATION
Zhou Q, Li X, Chang Y, Yu J, Luo W and Bai X (2023), Strong earthquake recurrence interval in the southern segment of the Red River Fault, southwestern China.
Front. Earth Sci. 11:1280787.
doi: 10.3389/feart.2023.1280787

Strong earthquake recurrence interval in the southern segment of the Red River Fault, southwestern China

Qingyun Zhou[1,2], Xi Li[3]*, Yuqiao Chang[1], Jiang Yu[1], Weidong Luo[1] and Xianfu Bai[1]

[1]Yunnan Earthquake Agency, Kunming, Yunnan, China, [2]Kunming Institute of Earthquake Forecast, China Earthquake Administration, Kunming, Yunnan, China, [3]School of Earth Science, Yunnan University, Kunming, China

Along the southeastern margin of the Tibetan Plateau, an important boundary fault, known as the Red River Fault (RRF), formed during the extrusion of mantle and lower crustal materials beneath the Tibetan Plateau. The characteristics of RRF activity are important for understanding the tectonic evolution of the southeastern margin of the Tibetan Plateau. There is less knowledge about the strong earthquake recurrence interval in the southern segment of the RRF than about its northern segment. In this study, based on the characteristics of the active tectonic landform, three paleoseismic trenches were excavated in Adipo Village north of Honghe County in the southern segment of the RRF. In these trenches, three paleoseismic events that occurred in the middle and late Holocene were identified. According to the ^{14}C dating results, these events were constrained to 785–504 BC, 26–492 AD, and 1,415–1857 AD. The average earthquake recurrence interval was determined to be approximately 960–1,320 a.

KEYWORDS

Red River Fault, SE Tibetan plateau, active fault, strong earthquake recurrence interval, paleoseismic events

1 Introduction

In the southeastern area of the eastern Himalayan syntaxis on the Tibetan Plateau, the Red River fault (RRF), which is over 1,000 km in total length, extends from Tibet to the South China Sea and is a major strike-slip fault in the Himalaya–Tibet Collision Zone (Figure 1) (Tapponnier et al., 1990; Zhang et al., 2002; Zhang et al., 2004). The RRF is a boundary fault between the Indochina and South China plates and is also the boundary of the Sichuan–Yunnan Block (SYB), which is the southeastward extrusion channel for mantle and crustal materials beneath the Tibetan Plateau. From a scientific perspective, studying the RRF in detail is important for further understanding the geodynamic processes occurring in the southeastern marginal region of the Tibetan Plateau (Wang et al., 1998; Gilley et al., 2003; Schoenbohm et al., 2005; Xuan et al., 2018; He et al., 2020; Yu et al., 2020).

The RRF in China can be divided into three sections by two locations, Juli and Dadoumen (Guo et al., 2001), namely, the northern segment, the middle segment, and the southern segment (Figure 1). Historically, two earthquakes above magnitude 7.0 and seven earthquakes in the magnitude range of 6.0–6.9 occurred in the RRF zone. All these earthquakes occurred in the northern segment of the RRF. There are no earthquake records for the southern segment of the RRF. Such a small number of earthquakes is significantly

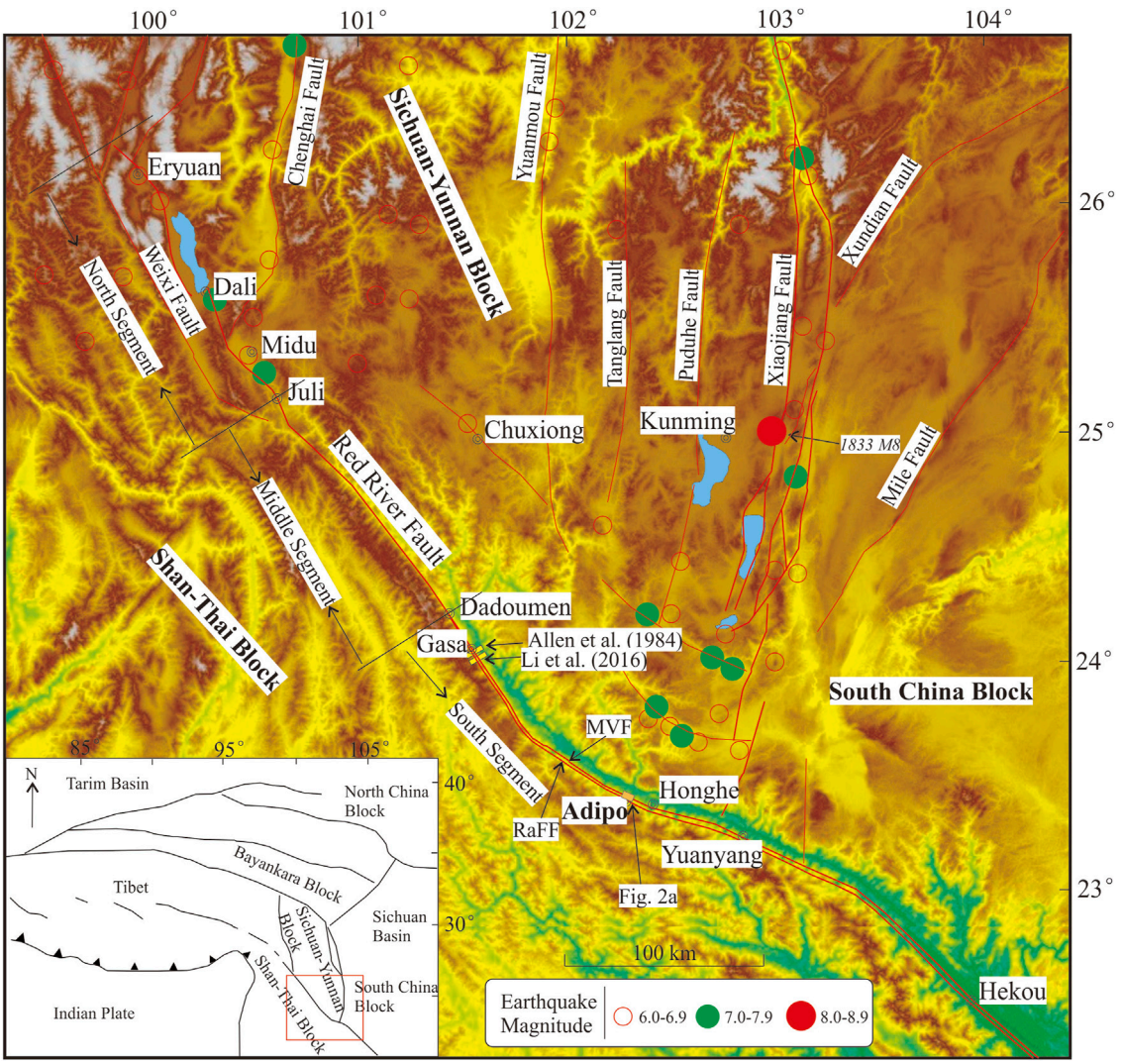

FIGURE 1
Tectonic map of the Red River Fault and its adjacent areas. The blue area indicates lakes. Yellow rectangles indicate locations of other trenches. Thick red lines indicate boundary faults of the SYB. Thin red lines indicate main faults in and around the SYB.

inconsistent with the important role of the RRF in the tectonic evolutionary process of the Tibetan Plateau. Currently, a consensus regarding the future seismic activity in the southern segment of the RRF remains elusive. Some researchers believe that the boundary effect of the RRF, which is a primary geotectonic boundary, has weakened and that no strong earthquakes will occur in the RRF zone in the future (Guo et al., 2001; Zhang et al., 2009; Shi et al., 2018). However, others argue that the RRF may be in an earthquake-preparation stage at present and remains at risk of strong earthquakes in the future (Allen et al., 1984; Li et al., 2016; Yin et al., 2018).

The reasonable assessment of the seismic risk of the RRF, particularly its southern segment, is important for reducing and mitigating disasters and has sociological significance. Accurate determination of the latest active period, strong earthquake recurrence interval, and slip rate is needed for assessing the seismic risk of the RRF. By measuring the dextral offset of the ancient drainage system as well as by estimating the time when the offset started, previous researchers determined a long-term average slip rate of 2–5 mm/a for the RRF zone (Allen et al., 1984; Replumaz et al., 2001; Schoenbohm et al., 2006; Chen, 2013). Compared with the values obtained using geological methods, the slip rate estimated based on cross-fault deformation and Global Positioning System measurements was relatively low at approximately 0.4–2 mm/a (Cong and Feigl, 1999; Feigl et al., 2003; Shen et al., 2005; Wang et al., 2008; Zuchiewicz and Cuong, 2009; Zhao et al., 2012; To et al., 2013; Hao et al., 2014; Zheng et al., 2017; Wang and Shen, 2020). However, it is difficult to evaluate the errors in the estimated slip rates. In addition, the long-term average slip rate is not necessarily consistent with the Holocene slip rate. Moreover, the surface slip rate is not necessarily the same as the underground slip rate. Previous researchers have presented relatively scant direct seismic and geological evidence to support their estimations of the latest active period and strong earthquake recurrence interval for the southern segment of the RRF. Trenches have only been excavated near Gasa (Figure 1). However, Gasa is less than 30 km from

Dadoumen, which separates the middle and northern segments of the RRF. Furthermore, the strike (325°) of the RRF at Gasa differs considerably from that (285°–310°) of most of the southern segment of the RRF. Thus, further research is required to determine whether the activity characteristics of the RRF near Gasa can represent those of the whole RRF.

In this study, combined with field investigation, trench sites were selected. Subsequently, three trenches were excavated in Adipo Village, Honghe County, in the southern segment of the RRF. Based on the analytical results of the trenches and ^{14}C dating, the strong earthquake recurrence interval on the southern segment of the RRF was investigated.

2 Method

The frequency of strong earthquakes ($M \geq 7$) on active faults is an important parameter to describe the risk of faults. The history of earthquake records on the Red River Fault is only approximately 1,200 years, while the recurrence of strong earthquakes on this fault is up to thousands of years. Therefore, it is necessary to use paleoseismic investigation methods (paleoseismology) to obtain the sequence of strong earthquake events that occur on this fault (McCalpin, 2009; Ran and Deng, 1999; Ran et al., 2012).

Paleoseismology is mainly divided into two aspects: stratigraphic deformation and geomorphological deformation. We use paleoseismic trenches to identify paleoseismicity and obtain the recurrence interval of strong earthquakes in the Red River Fault.

3 Geological settings

The Indian Plate has been continuously colliding with the Eurasian Plate since the Eocene. The vertical ascension of the materials in the collision zone between the two plates has resulted in the formation of the Tibetan Plateau. This process is also accompanied by the lateral extrusion of crustal and mantle materials. Due to the presence of a barrier (i.e., the hard Tarim Block) on the north side, mantle and lower crustal materials in the collision zone are extruded clockwise to the east and southeast. The collision between the materials extruded eastward and the Yangtze Block resulted in the formation of the Longmenshan Fault zone. The collision and compression between the materials extruded southeastward and the Indochina Block has led to the formation of the vast Southeast Asian inland deformation zone (SAIDZ) (Tapponnier and Molnar, 1976; Tapponnier et al., 2001). On the northern end of the SAIDZ and adjacent to the eastern Himalayan syntaxis, the SYB is enclosed by the RRF, the Xiaojiang Fault, and the Anning River Fault. The RRF is the southwestern boundary of the SYB as well as the boundary between the SYB and the Shan-Thai Block (Deng et al., 2002). Early ductile sinistral strike-slip shear movements occurred in the RRF zone 35–32 to 22 Ma before present (BP). The sinistral offset might have been as long as 700 km (Harrison et al., 1992; Leloup et al., 1995; Chen et al., 1996; Harrison et al., 1996; Wan et al., 1997; Zhang et al., 2009; Searle et al., 2010). Since the Pliocene, normal and dextral strike-slip movements have been the predominant forms of motion of the RRF (Ran et al., 1988; Guo et al., 1996; Trieu, 2003; Xiang et al., 2004; Xiang et al., 2007; Wang et al., 2011).

The northern segment of the RRF (from Eryuan to Midu) is spatially distributed in a complex pattern with many branch faults, but its activity characteristics are clear (e.g., the latest active period and strong earthquake recurrence interval) (Ran et al., 1988; Guo et al., 2001). The spatial distribution of the middle segment of the Red River Fault (from Midu to Dadoumen) is simple, with only one fault, and its width is relatively small. The southern segment of the RRF (from Dadoumen to Hekou) is spatially distributed in a relatively simple pattern and extends along the Red River Valley in approximately the southeastern direction. In addition, the southern segment of the RRF consists of two nearly parallel faults, namely, the Range Front Fault (RaFF) and the Middle Valley Fault (MVF), but the characteristics of its activity remain unclear. Compressional thrusting is the predominant form of motion in the RaFF zone in the early and normal uplifting in the later stages, whereas dextral shear movements are relatively weak in the RaFF zone. The MVF is characterized by steep dips, notable shear cleavage zones, and prominent dextral shear deformation (e.g., creep and traction) in Miocene sandy conglomerate strata (Replumaz et al., 2001; Schoenbohm et al., 2006; Li et al., 2016). Because the MVF has clearer linear features in satellite images and stronger activity in terms of tectonic landforms, researchers are focusing on the activity characteristics of the MVF. The fault being investigated in this article is the MVF.

4 Investigation of paleoearthquakes that occurred near Honghe County

4.1 Trench sites

Trenching is one of the most direct and effective methods used to study strong earthquake recurrence intervals in active fault zones. Because the excavation depth is limited, trenches should be excavated at sites with low Quaternary deposition rates. Very high Quaternary deposition and erosion rates are often found in the southern segment of the RRF, particularly south of Yuanjiang County, due to heavy precipitation and the presence of high mountains and narrow gullies. This is also results in a failure to identify seismic events in paleoseismic trenches that were previously excavated in the section of the RRF south of Yuanjiang County. In this study, trenches were excavated in the fault trough on the hillside of Adipo Village, located 12 km northwest of Honghe County (Figure 1). A relatively dry climate as well as a relatively small catchment area led to relatively low Quaternary deposition rates at the trench sites. This provided favorable conditions for recording more paleoseismic events.

Three trenches were excavated based on the characteristics of the active tectonic landform in the field (Figure 2A, B) to determine the latest active period of the southern segment of the RRF and the recurrence of paleoearthquakes since the Holocene and to accurately assess the potential seismic risk to the southern segment of the RRF. Trench 1, approximately 75 m in length, extended across the fault trough with a wide and gentle bottom. Trench 2, approximately 40 m in length, stretches through a small reverse scarp on the hill ridge. Trench 3, approximately 75 m in length, was located next to a

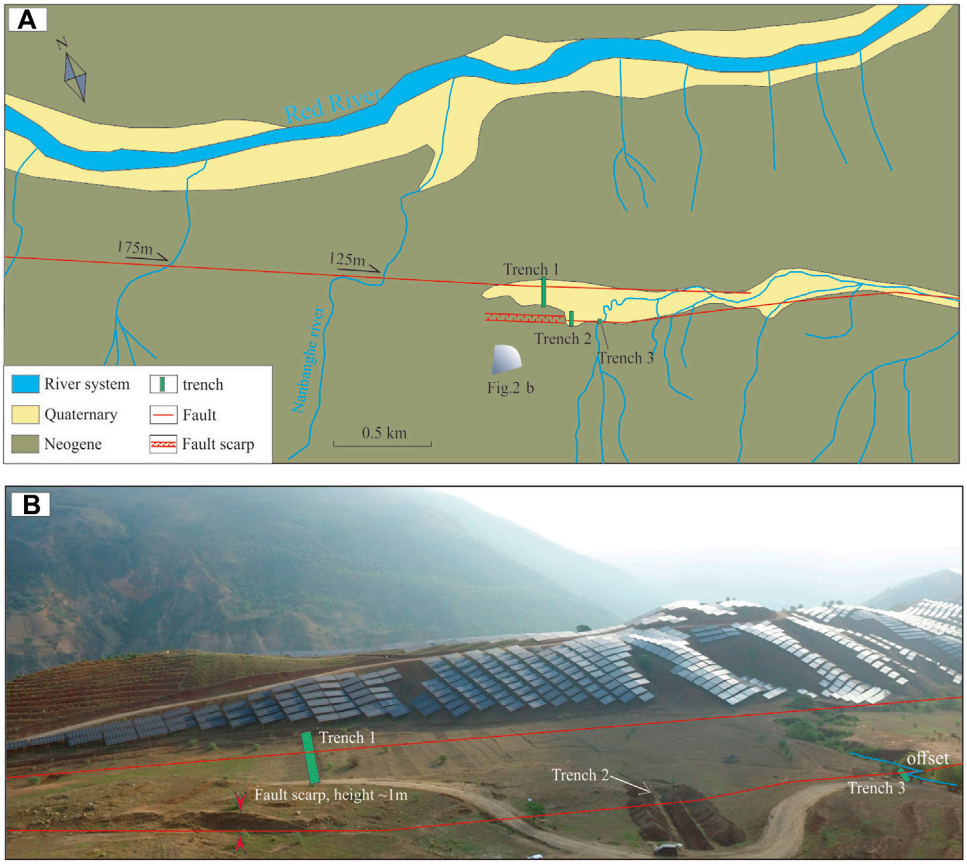

FIGURE 2
(A) Geological structure environment near the trenches. The gradient fan indicates the photo position and direction of Figure 2B. **(B)** Trench layout photo (viewed toward the east). The length of the solar panel in this photo is 10 m. The blue line indicates the gully. Linear ridges and fault trough can be observed in this photo.

gully dislocation. An analysis of the dating results and paleoseismic events shows that these three trenches revealed multiple paleoseismic events.

4.2 Investigation of paleoseismic events based on trench 1

4.2.1 Stratigraphic sequence

Spanning the entire wide fault trough, trench 1 was approximately 75 m in total length, approximately 4 m in average depth, and approximately 5 and 1 m in width at the top and bottom, respectively. In this paper, only 11 Quaternary strata closely related to paleoseismic events and from which charcoal samples were collected are described. These strata exhibit the characteristics of deposition in still-water-like settings and show a notable sedimentary rhythm (Figure 3). These 11 strata are denoted, from old to young, by U1–U11 (see Table 1 for details).

4.2.2 Analysis of paleoseismic events

Paleoseismic events were primarily found in the middle and northern segments of trench 1 (Figure 3). The paleoseismic events identified on the SE and NW walls of trench 1 were similar. Credible features for identifying Quaternary strike-slip faults include tectonic wedges, pore fillings, and sand veins. Based on these features of paleoseismic events in strike-slip faults, clear indications of three paleoseismic events (TC1-E1, TC1-E2, and TC1-E3) were identified in trench 1 (Figure 4). The stratigraphic evidence of these three paleoseismic events is detailed as follows:

Event TC1-E1: Indications of this event were found at multiple locations in trench 1, e.g., at faults F1, F4, F5 and F7 (Figures 4A, C, D, E) on the NW wall and at faults F16, F17, F18, F19 and F21 (Figures 4I–L) on the SE wall. With steep dips that mostly exceed 80°, these faults offset unit U1, fill unit U2 and are overlaid by unit U3. Cracks 1–3 cm in length are present at most of the fracture surfaces and are filled with the yellow sand of unit U2, forming sand veins. Thus, it is inferred that event TC1-E1 occurred after the formation of unit U2 and before the formation of unit U3.

Event TC1-E2: Manifestations of this event, mostly in the form of tectonic wedges, were found at faults F2, F3, F6 and F8 (Figures 4A, B, D, F) on the NW wall of trench 1 and at faults F11, F12, F13, F14, F15 and F20 (Figures 4G–I, K) on the SE wall of trench 1. The faults formed as a result of event TC1-E2 have relatively steep dips that are slightly gentler than those of the faults formed as a result of event TC1-E1. The faults formed from event TC1-E2 offset unit U4 and those beneath it fill unit U5 and are overlaid by unit U6.

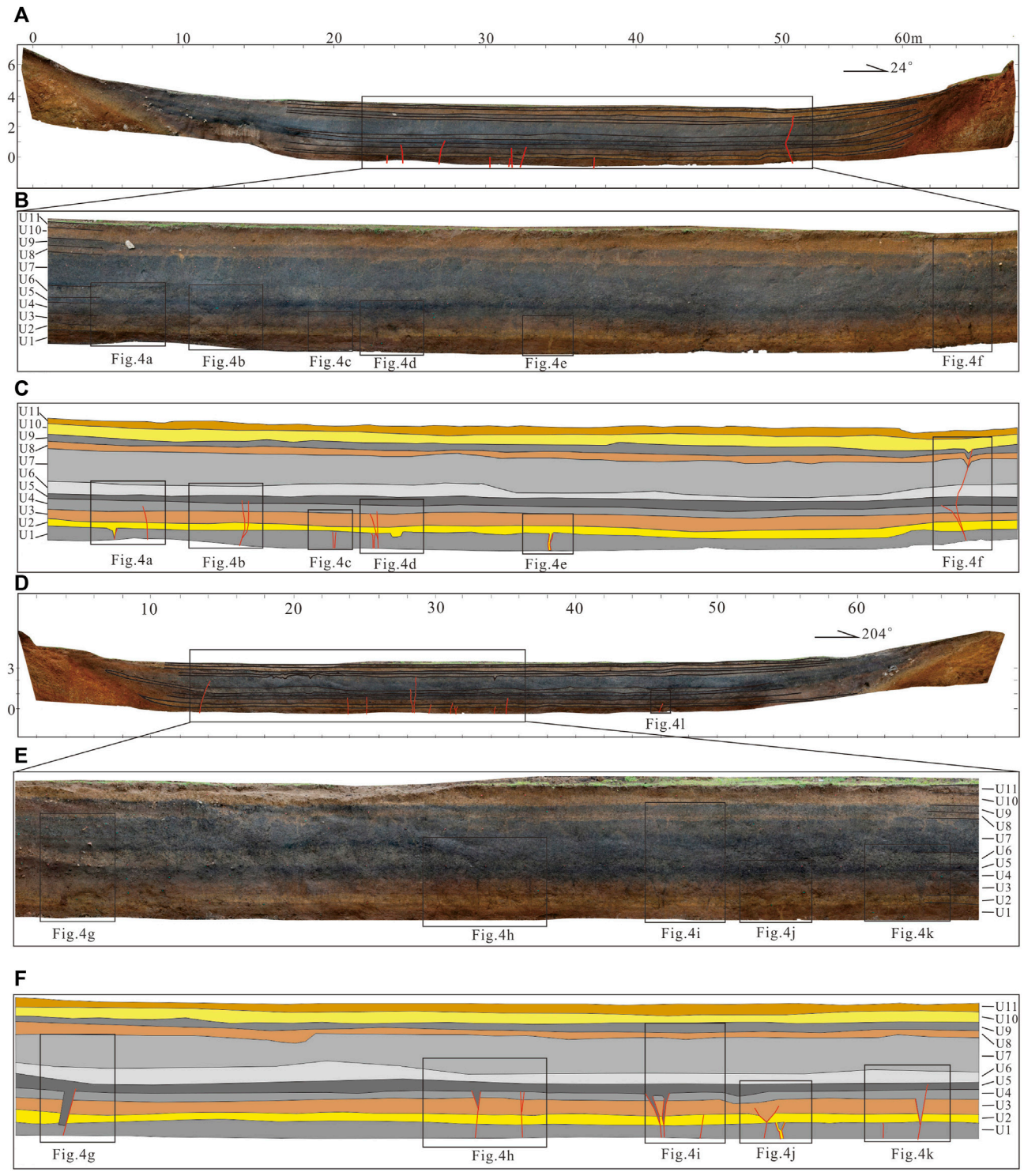

FIGURE 3
Simplified schematic diagrams of the strata in trench 1: **(A–C)** northwest (NW) wall; **(D–F)** southeast (SE) wall.

Thus, it is inferred that event TC1-E2 occurred after the formation of unit U5 and before the formation of unit U6.

Event TC1-E3: Event TC1-E3 is the latest and most complex paleoseismic event identified in trench 1. Evidence of this event was found only at fault F9 (in Figure 4F) on the NW wall of trench 1. Fault F9 offsets unit U9, fills unit U10 in a tectonic wedge, and is overlaid by unit U11 (gravel particles approximately 3 cm in size were found at the bottom of the tectonic wedge and presumably might have been formed by the colluvial gravel on the surface after the formation of the tectonic wedge). At the latest, this event likely occurred during the formation of the portion of unit U10. Thus, it is inferred that event TC1-E3

TABLE 1 Unit description from trench 1 exposures in Adipo Village.

Unit no.	Description
U1	A brown sand unit that contains brown and gray interbeds and is rich in carbon content
U2	A yellow clayey silt unit that has low clay content and is intercalated with thin grayish-yellow and grayish-brown layers. This unit is a signature unit identified in trench 1
U3	A brown sandy clay unit that has low sand content and contains a small amount of gravel with a particle size of 0.5–2 cm
U4	A black gravelly clay unit, where the gravel is somewhat large (with a particle size of 1–3 cm) at the toe on each end and generally exhibits particle sizes smaller than 1 cm in the middle
U5	A sandy clay unit that has a high sand content and contains gravel with a particle size of 2–5 cm in local areas
U6	A grayish-white clay unit that contains a small amount of gravel with a particle size of 0.5–4 cm at the toe on each end
U7	A black sandy clay unit that contains sporadic boulders approximately 5 cm in size in local areas
U8	A yellow clay unit that contains a small amount of gravel with very round particles sized 3–5 cm at the toe on each end
U9	A silty clay unit that contains gravel with very round particles sized 3–5 cm at the toe on each end
U10	A 30-cm-thick yellow silty clay unit
U11	A gray clay unit that is the plow layer with 10–15 cm thickness

occurred after the formation of unit U9 and before the formation of unit U10.

We rearranged the 21 faults in trench 1 based on the relationships between them and the strata (Figure 5). According to Figures 5, 9 faults are related to event TC1-E1, 11 faults are related to event TC1-E2, and 1 fault is related to event TC1-E3. There are 3 paleoseismic events in this trench.

4.2.3 Chronological constraints on paleoseismic events

Many charcoal samples were collected from trench 1, of which 14 were sent to Beta Analytic (US) for accelerator mass spectrometry dating. Seven of the 14 samples contained sufficient charcoal, from which definitive chronological information was extracted (see Table 2 for details).

Event TC1-E1: As mentioned above, this event occurred after the formation of unit U2 and before the formation of unit U3. Thus, the ages of carbon (C) sample TC1-244 collected from unit U2 and C sample TC1-245 collected from unit U3 are used as the lower and upper age limits of this event, respectively. In other words, event TC1-E1 was constrained to 785–504 BC (Figure 9).

Event TC1-E2: This event occurred after the formation of unit U5 and before the formation of unit U6. Thus, the ages of sample TC1-212 collected from unit U5 and sample TC1-268 collected from unit U6 are used as the lower and upper age limits of this event, respectively. In other words, event TC1-E2 was constrained to 359 BC-492 AD (Figure 9).

Event TC1-E3: This event occurred after the formation of unit U9 and before the formation of the portion of unit U10. Thus, the ages of sample TC1-256 collected from unit U9 and sample TC1-253 collected from unit U10 are used as the lower and upper age limits of this event, respectively. In other words, event TC1-E3 was constrained to 1,415–1857 AD (Figure 9). Plant root systems were found in unit U10. While areas of unit U10 relatively abundant in plant root systems were deliberately avoided during the sampling process, the age of sample TC1-253 may have been underestimated by dating analysis.

4.3 Investigation of the paleoseismic events identified in trench 2

After trench 1 was cleared, Yongkang Ran, a distinguished professor in paleoseismology, was invited to consult on site. During this process, a small fault scarp and a trough valley approximately 30 m southwest of trench 1 were discovered (shown in Figure 2B). In addition, an outcropping profile of a fault was found approximately 150 m southeast of trench 1, and a gully was found along the strike of fault (Figure 2B). Thus, another trench (trench 2) was excavated in a section with relatively developed Quaternary strata selected on the line connecting the fault scarp and the offset. More faults and indications of paleoseismic events were found on the NW wall of trench 2 than on the SE wall. Thus, focus was placed on the NW wall, which contained relatively rich fracture-surface information, as well as dating of the samples collected from the NW wall (Figure 6A, B).

4.3.1 Stratigraphic sequence

Striking north–east overall, trench 2 was approximately 40 m in length, 4 m in depth, and 5 and 1 m in width at the top and bottom, respectively. Apart from the weathered bedrock, a total of eight Quaternary strata were identified in trench 2. Similar to trench 1, a relatively notable sedimentary rhythm was found in trench 2. The weathered bedrock is denoted by U0. The eight Quaternary strata are denoted from old to young by U1–U8 (see Table 3 for details).

4.3.2 Analysis of paleoseismic events

Two paleoseismic events were identified in the Quaternary strata in trench 2. The older and younger events are referred to as TC2-E1 and TC2-E2, respectively. Based on the identification markers for paleoseismic events in strike-slip faults, the two paleoseismic events identified in trench 2 as well as the relevant stratigraphic evidence are detailed below (Figure 7).

Event TC2-E1: Similar manifestations were found at faults F1 and F2 in Figure 7A. These two faults offset unit U1, forming tectonic wedges that are filled by the materials of unit U2. This

10.3389/feart.2023.1280787

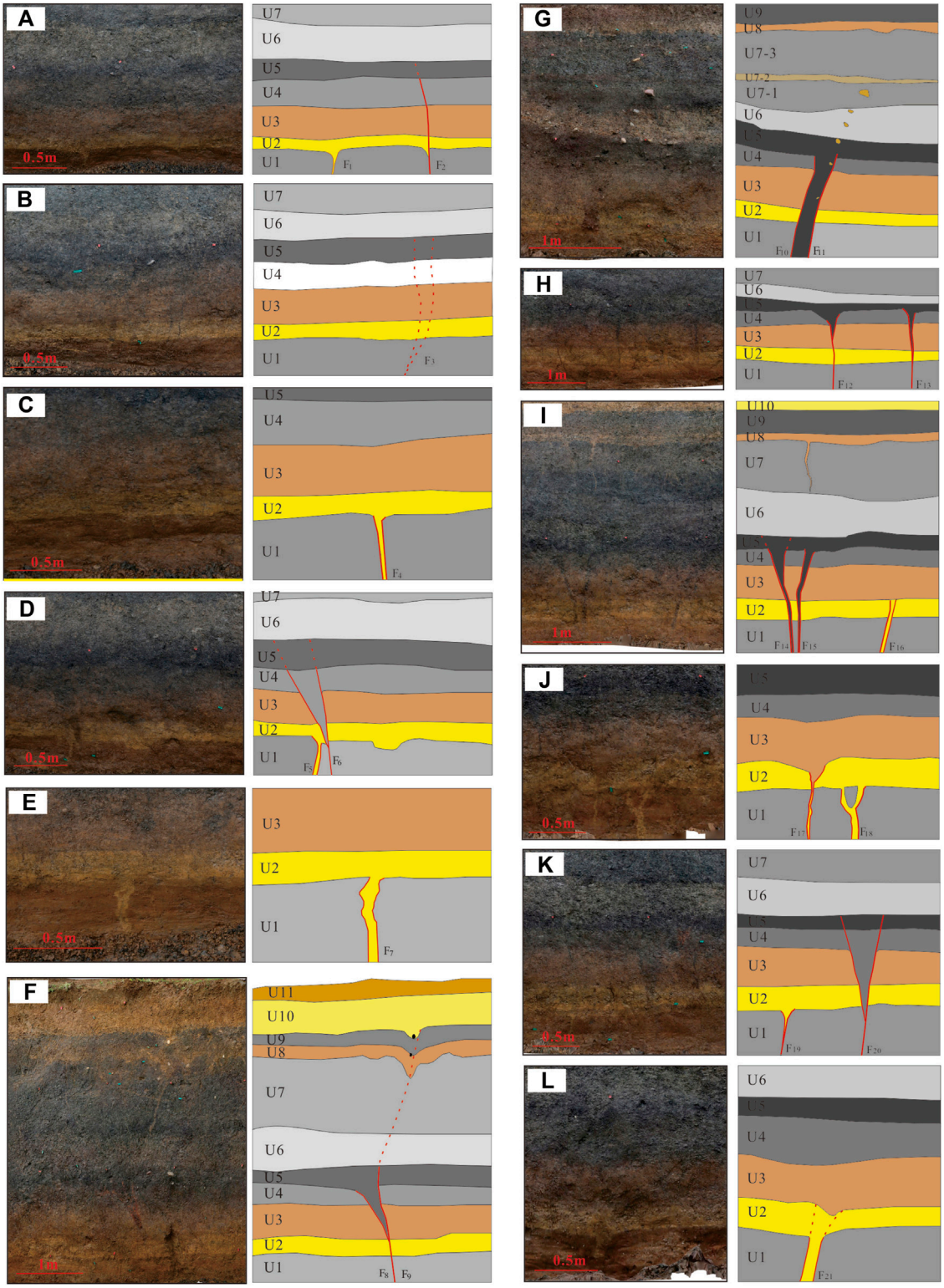

FIGURE 4
Images of some local areas of the two walls of trench 1 and their interpretation (the left and right images of each set are the original photograph and its geological interpretation, respectively; the red solid lines and red dashed lines indicate faults and inferred faults, respectively; see Figure 3 for the locations of the areas where the photographs were taken). **(A–F)** northwest (NW) wall, **(G–L)** southeast (SE) wall.

finding suggests that event TC2-E1 occurred after the formation of unit U2. No notable traces of faults are present in unit U3, indicating that event TC2-E1 occurred before the formation of unit U3.

Event TC2-E2: In Figure 7B, Faults F3 and F4 offset unit U5, forming 2 tectonic wedges approximately 60 cm in height that are filled with the materials of unit U7. In addition, Faults F3 and

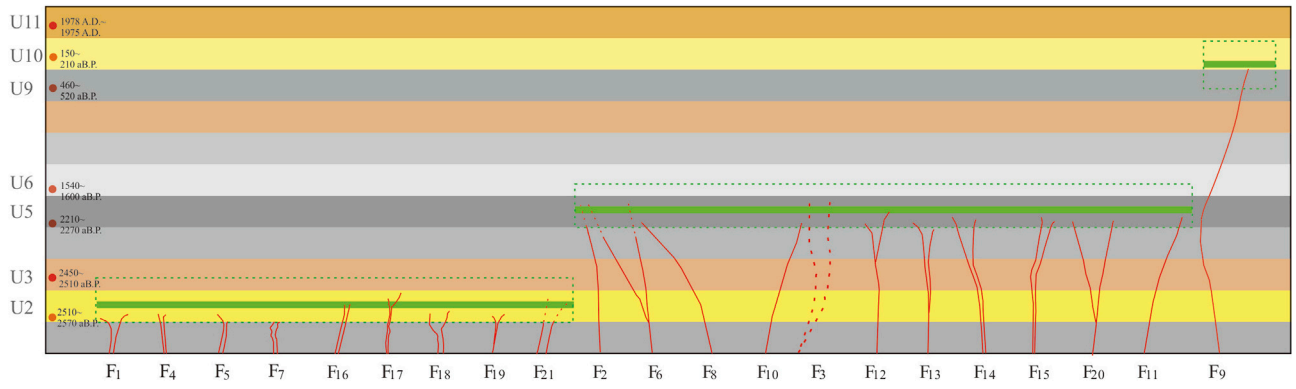

FIGURE 5
Rearranged faults in trench 1. Red lines indicate faults in trench 1, green thick lines indicate paleoseismic events, and green dashed lines indicate their uncertainties. Red small circles and the number to the right indicate sample location and dating results. Colored horizontal strips indicate the strata in trench 1.

TABLE 2 Sample testing results.

Sample no.	Laboratory no.	Dating result (a BP)	Calibration result[a]		Sample description	Sample location
			95.4%	68.3%		
TC1-221	509,129	1978 AD	1978–1979AD	1979AD	Carbon	U11
TC1-253	509,131	180 ± 30	1,655–1950AD	1,666–1950AD	Carbon	U10
TC1-256	510,876	490 ± 30	1404–1452AD	1417–1442AD	Carbon	U9
TC1-268	553,466	1,570 ± 30	425–565AD	435–547AD	Carbon	U6
TC1-212	550,556	2,240 ± 30	390–202BC	381–210BC	Carbon	U5
TC1-244	515,002	2,540 ± 30	796–547BC	790–590BC	Carbon	U2
TC1-245	515,003	2,480 ± 30	772–476BC	756–543BC	Carbon	U3
TC2-005	563,321	2,610 ± 30	821–769BC	807–786BC	Carbon	U2
TC2-014	563,322	1990 ± 30	46BC-117AD	37BC-64AD	Carbon	U5
TC2-038	563,323	1,200 ± 30	706–945AD	782–881AD	Carbon	U6
ADP-W1-11	510,874	180 ± 30	1,655–1950AD	1,666–1950AD	Carbon	

[a]Calibrated with OxCal v4.4.4 using the calibration curve of IntCal20 (Reimer et al., 2020).

F4 offset unit U4 and U3-2 without vertical displacement. This finding suggests that strike-slip faulting was the main form of motion of this event. From the shape of the lower boundary of unit U3-2 and U4, in addition to the strike-slip component, this event may also have the property of tension. The fact that both tectonic wedges are filled with the materials of unit U5 in Figure 7B suggests that event TC2-E2 occurred after the formation of unit U5. No notable traces of faults are present in unit U7, indicating that event TC2-E2 occurred before the formation of unit U7.

4.3.3 Chronological constraints on paleoseismic events

A total of five ^{14}C samples were sent to Beta Analytic (US) for dating. Three of the five samples contained sufficient charcoal, from which definitive chronological information was extracted (see Table 2 for details). It is inferred from the dating results that events TC2-E1 and TC2-E2 were constrained to 803 BC-16 AD and 26–856 AD, respectively.

4.4 Trench 3 at the edge of the gully

Trench 3 was discovered 75 m southeast of trench 2 along the extension of the fault (Figure 8). The relative locations of the fault outcrop and trench 2 are shown in Figure 2. A fracture zone, approximately 1.1 m in width, was found between fault 1 and fault 2 in Figure 8C. This wide fracture zone suggests that historically, this site fractured multiple times. The fault revealed by the trench should be the main fault of the RRF.

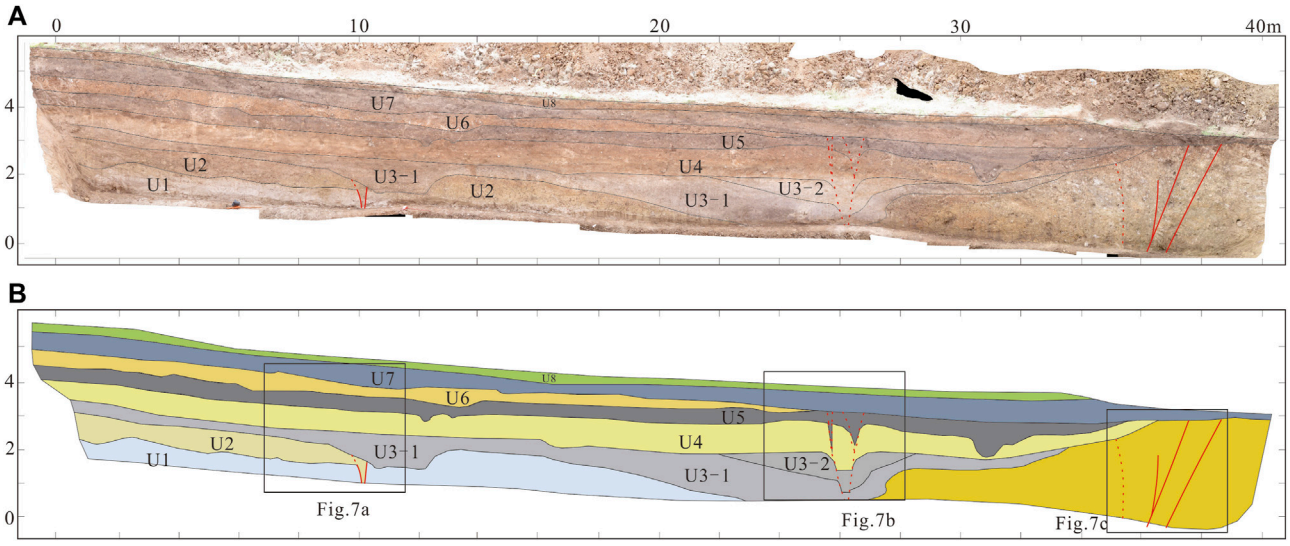

FIGURE 6
Simplified schematic diagrams of the strata in the NW wall of trench 2. **(A)** photograph, **(B)** interpretation.

TABLE 3 Unit description from trench 2 exposures in Adipo Village.

Unit no.	Description
U0	A unit formed from the weathering of sandy conglomerates that contains clay in local areas. The gravel in this unit is poorly rounded and has a particle size of approximately 0.5–5 cm
U1	A grayish-white sand unit that is low in clay content but contains massive amounts of clay in local areas
U2	A grayish-yellow to grayish-brown clayey silt unit, 0.6–0.8 m in thickness, that is high in sand content at the toes and contains poorly rounded and sorted gravel
U3-1	A gray to grayish-white clay unit, 0.3–1.3 m in thickness, that contains brown banded interlayers as well as gravel (with a particle size of 0.2–1 cm) and boulders in local areas
U3-2	A grayish-white to gray sandy clay unit, 0.3–1.3 m in thickness, that exhibits lacustrine sedimentary facies and contains sandy gravel with a particle size of 0.2–1 cm at the bottom
U4	A grayish-yellow clay unit, approximately 0.7 m in thickness, that contains gravel with a particle size of 2–10 cm in local areas
U5	A grayish-black muddy clay unit, 0.5–0.7 m in thickness, that contains relatively rounded gravel with a particle size of 0.2–5 cm
U6	A light-yellow clay unit, 0.2–0.5 m in thickness, that contains a large amount of gravel (with a particle size of 0.2–2 cm) and sand
U7	A gray muddy clay unit, 0.3–0.6 m in thickness, that contains granules 0.1–1 cm in size
U8	A yellow loam unit approximately 0.1 m in thickness

4.4.1 Stratigraphic sequence

Trench 3 was approximately 6 m in length and 3 m in height (Figure 8A). Apart from the fracture zone, a total of eight strata were identified in the profile. Unit U1 was found to be solidified with highly weathered gravel. No Quaternary sedimentary characteristics were discovered in unit U1. Thus, it is inferred that unit U1 might have been formed as a result of the weathering of bedrock. The eight strata are denoted from old to young by U1–U8 (see Table 4 for details).

4.4.2 Paleoseismic events

At least two paleoseismic events were revealed by this trench. In the first event (W1-E1), fault F1 offset unit U3, forming a colluvial wedge (Figure 8B). As demonstrated in the interpreted image (Figure 8C), the materials comprising the colluvial wedge are lighter in color and contain gravel larger in both quantity and particle size than that comprising the fracture zone. In addition, some small tectonic wedges were found near the fault plane (Figure 8D). This finding suggests that the formation of the colluvial wedge was related to the paleoseismic event.

During the second event (W1-E2), fault F2 offset unit U5 by 25 cm. A series of small vertical cleavage zones was found in unit U5 upward along the fault. Units U5 and U7 may be in fault contact.

Unfortunately, no ^{14}C samples were collected from the key units (i.e., units U3 and U5 as well as the colluvial wedge). ^{14}C samples were collected only from unit U7. The samples collected from the bottom of unit U7 were dated to 1,652–1950 AD. This

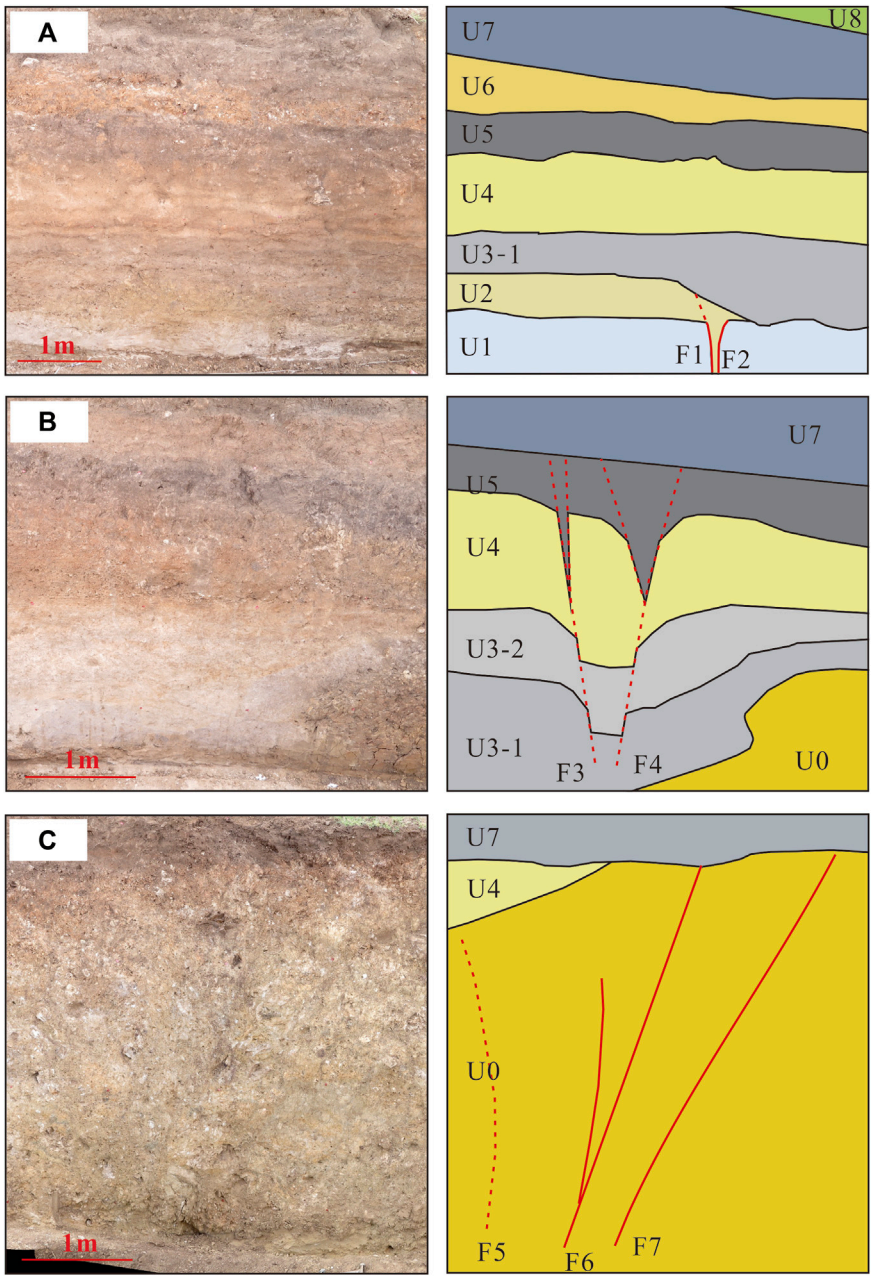

FIGURE 7
Images of some local areas of trench 2 excavated in Adipo Village and their interpretation. **(A)** west part of trench, **(B)** middle part of trench, **(C)** east part of trench.

estimated age is too young, which may be due to the presence of plant root systems.

5 Discussion

5.1 Comparative analysis of the paleoseismic events identified in the two trenches

Paleoseismic events of the two trenches are shown in Figure 9. Events TC1-E1 and TC2-E1 may be the same event. First, similar manifestations of the two events were found in the fault. Specifically, they both resulted in the formation of cracks 1–3 cm in length that were filled with overlying materials. Second, the relevant cut, filled, and overlying strata are similar in sedimentary rhythm and composition. The cut units (unit U1 for event TC1-E1 and unit U1 for event TC2-E1) are both sand units. The filled units (unit U2 for event TC1-E1 and unit U2 for event TC2-E1) are both yellow silt units. The overlying units (unit U3 for event TC1-E1 and unit U3 for event TC2-E1) are both clay units. Third, the chronological results for the filled units are similar. Based on this analysis, it is believed that events TC1-E1 and TC2-E1 are the same paleoseismic event, so the overlapping part of the occurrence time, 785–504 BC, is the actual occurrence time.

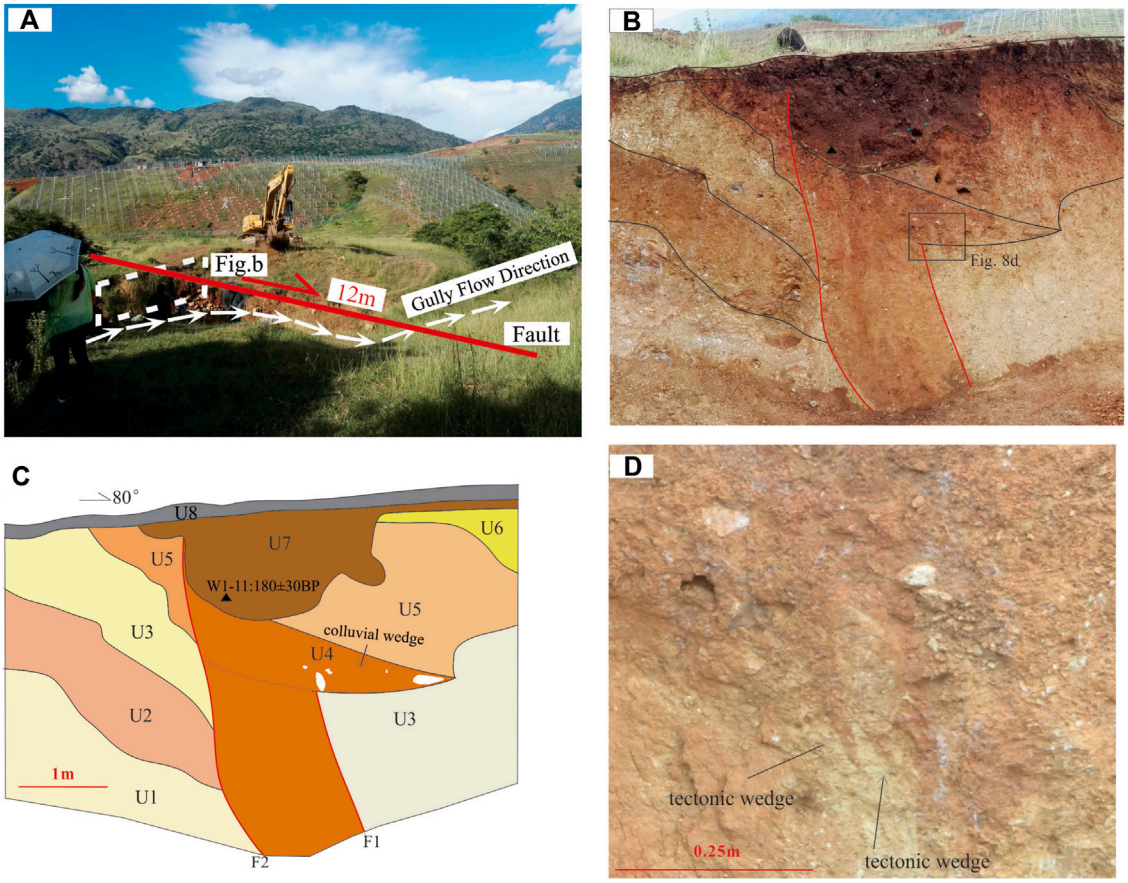

FIGURE 8
Images of the NW wall of trench 3. **(A)** environment, **(B)** photograph, **(C)** interpretation, **(D)** photo of tectonic wedge (Figure 8B indicate its location).

TABLE 4 Unit description from trench 3 near the gully.

Unit no.	Description
U1	A slightly solidified grayish-white sandy gravel unit that contains a small amount of clay and highly weathered gravel and is inferred to have formed as a result of bedrock weathering
U2	A brownish-yellow clay unit that is intercalated with a small amount of grayish-white gravel with a particle size of 0.5–1 cm
U3	A grayish-white to light-yellow clay unit that contains a large amount of angular gravel with a particle size of 0.1–2 cm
U4	Colluvial wedge
U5	A light-brown clay unit that contains a large amount of relatively uniformly distributed gravel and angular gravel with a particle size of 0.1–1 cm
U6	A gray sand-bearing clay unit
U7	A dark-brown to dark-gray clay unit that contains C and is abundant in plant root systems
U8	A grayish-black loam unit

Comparably, events TC1-E2 and TC2-E2 are also similar in terms of manifestations in the fault, the composition of the filled and overlying units, and the chronological results. Based on this analysis, it is believed that these two events are the same paleoseismic event, which occurred at 26–492 AD.

Event TC1-E3 was only identified in trench 1. No direct evidence of this event was found in trench 2. In Figure 2, the fault line connecting the reverse scarp and the gully intersects with trench 2 at its northeast end. Faults (F6 and F7 in Figure 7C) were found near the point of intersection. Because these faults developed in the

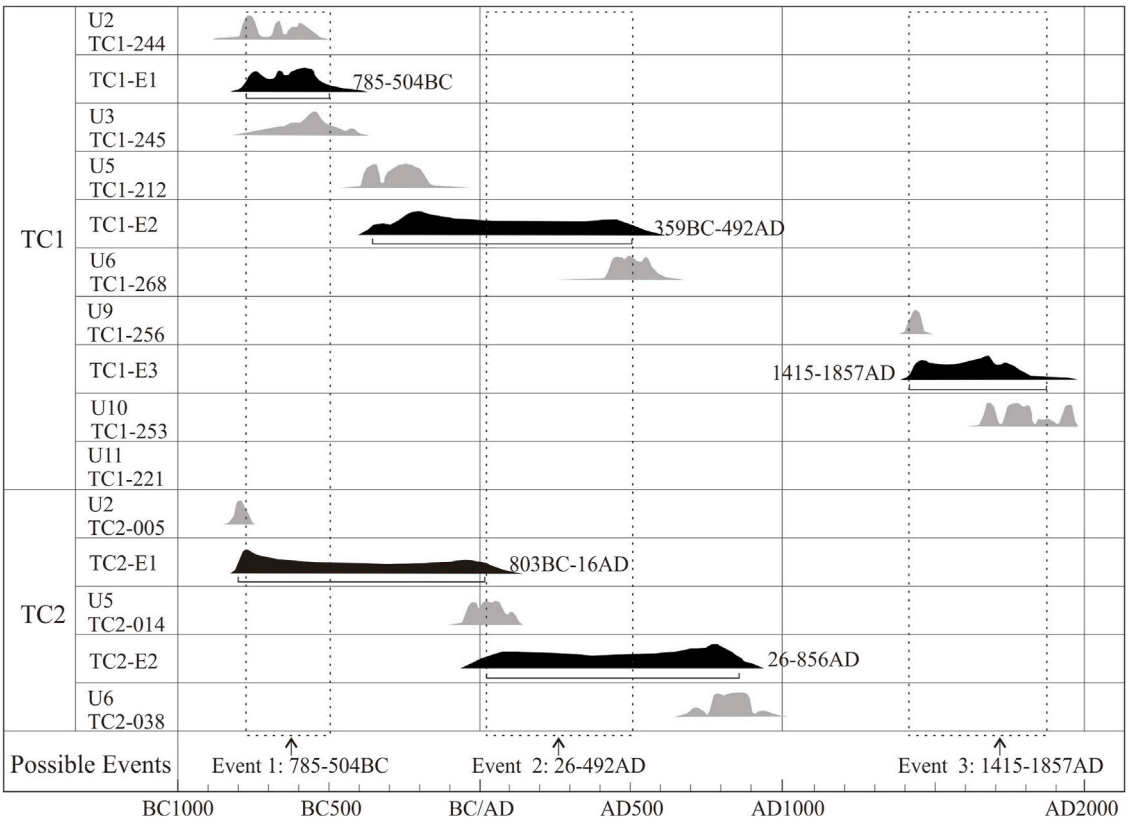

FIGURE 9
Time ranges of event occurrence in trench 1 and trench 2. Dashed boxes indicate the time ranges of 3 paleoseismic events. The gray areas indicate the dating results of the units. The black areas indicate the time ranges of paleoseismic events. Calibration was conducted with OxCal v4.4.4 using the calibration curve of IntCal20 (Reimer et al., 2020).

weathered bedrock layer, it is impossible to quantitatively analyze them based on the relationship between the offset and overlying units or the chronological dating results. This may be the primary reason why event TC1-E3 was not identified in trench 2.

5.2 Strong earthquake recurrence interval near Honghe County in the southern segment of the RRF

In a trench excavated near Gasa approximately 100 km northwest of Adipo, Allen et al. (1984) found evidence of 4 paleoseismic events, of which these events were Holocene seismic events above magnitude 7. However, this finding lacks support from quantitative dating data. Li et al. (2016) found indications of three paleoseismic events, which occurred 1,250–1730 AD, 240–580 AD, and 1700–650 BC, in two trenches excavated near Gasa. Shi et al. (2018) noted that two to three paleoearthquakes might have occurred near Gasa over the past 13,500 years.

In this study, three paleoseismic events were identified in two large trenches excavated in Adipo in the southern segment of the RRF based on the dating results from the many charcoal samples collected. These three paleoseismic events were constrained to 1,415–1857 AD, 26–492 AD, and 785–504 BC. Paleoseismic event occurrence times in this study and in Li et al. (2016) are combined for comparison (Figure 10). The occurrence times of the three paleoseismic events coincide well. We calculated the average dates of their overlapping parts, and the results were 718 BC, 366 AD, and 1491 AD. From this aspect, the average recurrence interval of the three events was 960–1,320 a.

5.3 Correspondence between historical earthquake records and paleoearthquakes

Some researchers believe that no destructive earthquakes have occurred in the southern segment of the RRF in the past 2,000 years due to a lack of historical earthquake records (Shi et al., 2018). In fact, the earliest recorded earthquake in Yunnan Province took place at AD 886 in Dali. There are records of only two earthquakes in Baoshan and Dali in the ensuing 400 years. Many earthquakes that occurred in Dali were not recorded, despite its historical importance as the political, cultural, and economic center in Yunnan. This recording failure would only be worse for the more remote Red River area. Thus, of the three paleoearthquakes identified in the trenches in Adipo, only the latest one might have been recorded.

There are often errors in the magnitude and location of historical earthquakes, particularly those that occurred in the remote regions of Yunnan, due to sparse settlements. Paleoearthquake TC1-E3 might have

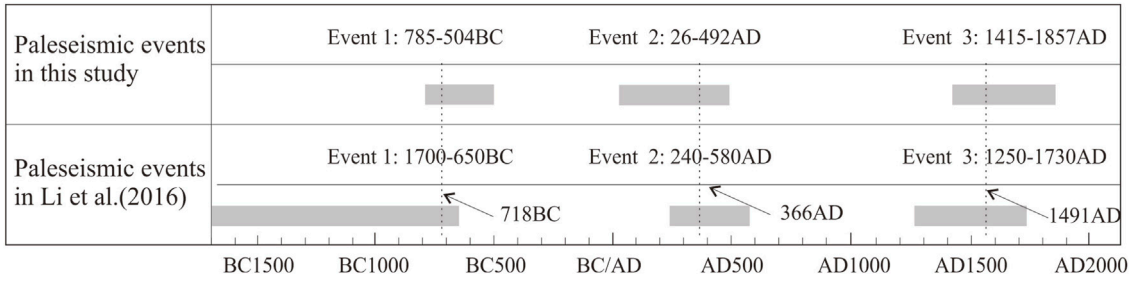

FIGURE 10
Comparison of paleoseismic event occurrence times in this study and in Li et al. (2016). Dashed lines indicate the average date of the overlapping parts.

TABLE 5 List of historical earthquakes near Jianshui that may be related to event TC1-E3.

No.	Date	Location	Magnitude	Near-field (Jianshui) damage	Far-field damage
E1	04/08/ 1,466	Jianshui	5 1/2	The city wall was damaged over a length of more than 660 m	None
E2	08/18/ 1,539	Jianshui	5 1/2	Some residents were crushed to death	Felt in Chuxiong and Luxi
E3	11/30/ 1,606	Jianshui	6 3/4	The city walls, temples, and government and residential buildings were all destroyed. The survivors slept in the open. Thousands perished	Felt in Mi'le

been recorded. Historically, Jianshui County was the regional political, cultural, and economic center closest to the southern segment of the RRF. The earliest recorded earthquake in Jianshui County occurred on 8 April 1,446, with a magnitude of 5.5. This record is the earliest historical earthquake record for the region along the southern segment of the RRF. Table 5 summarizes the historical earthquakes that occurred in Jianshui during 1,446–1800 AD. As demonstrated in Table 5, earthquakes E1 and E3 had similar near-field characteristics. Both of these earthquakes caused severe damage in the near-field area but almost no damage in the far-field area. Earthquake E2 was felt in Chuxiong and Luxi. Chuxiong was approximately 205 km away from Jianshui. Evidently, a magnitude 5.5 earthquake cannot be felt at a location 205 km away from its epicenter. Assuming that this earthquake occurred in the Gasa–Adipo region with a magnitude of 7.5, its intensity would have been 6–7 in Jianshui County (based on the damage caused by historical earthquakes above magnitude 7 that occurred within the province (e.g., the earthquake with a magnitude ≥7 that occurred in Yiliang in 1,500) as well as by taking earthquake rupture scaling into consideration) and 5 in Chuxiong. This finding is close to the historical records of the damage caused by this earthquake. Based on this analysis, it is believed that paleoearthquake TC1-E3 (i.e., the 1,539 Jianshui earthquake) was recorded. The magnitude of this earthquake might have been approximately 7.5.

6 Conclusion

In this study, three paleoseismic events were identified in the paleoseismic trenches excavated in Adipo Village, Honghe County in the southern segment of the RRF. According to the ^{14}C dating results, these events were constrained to 785–504 BC, 26–492 AD, and 1,415–1857 AD. The average recurrence interval of the three events was 960–1,320 a. This finding suggests that the southern segment of the RRF is an active Holocene fault zone with a short strong earthquake recurrence interval, long elapsed time since the last strong earthquake, and at high risk for seismic activity.

An analysis of the damage caused by recorded historical earthquakes shows that the youngest paleoearthquake (TC1-E3) identified in the trenches is the 1,539 Jianshui earthquake. The rupture length and magnitude of this earthquake may have been over 100 km and approximately 7.5, respectively.

Data availability statement

The original contributions presented in the study are included in the article/Supplementary material, further inquiries can be directed to the corresponding author.

Author contributions

QZ: Investigation, Methodology, Writing–original draft. XL: Funding acquisition, Investigation, Writing–review and editing. YC: Investigation, Writing–original draft. JY: Investigation, Writing–original draft. WL: Investigation, Writing–original draft. XB: Investigation, Writing–original draft.

Funding

The author(s) declare financial support was received for the research, authorship, and/or publication of this article. The work reported in this paper was supported by the Key Research and Development Plan of Yunnan Province (No. 202203AC100003), the Science for Earthquake Resilience of China Earthquake Administration (XH19040) and the Young and Middle-aged Academic Leaders Reserve Talent Project of Yunnan Province (202005AC160002).

Acknowledgments

We thank the Seismological Bureau of Honghe County for helping in field work and gathering data on historical earthquakes.

Conflict of interest

The authors declare that the research was conducted in the absence of any commercial or financial relationships that could be construed as a potential conflict of interest.

Publisher's note

All claims expressed in this article are solely those of the authors and do not necessarily represent those of their affiliated organizations, or those of the publisher, the editors and the reviewers. Any product that may be evaluated in this article, or claim that may be made by its manufacturer, is not guaranteed or endorsed by the publisher.

References

Allen, C. R., Gillepsie, A. R., Han, Y., Sieh, K. E., Zhang, B. C., and Zhu, C. N. (1984). Red River and associated faults, Yunnan Province, China: Quaternary geology, slip rates, and seismic hazard. *Geol. Soc. Am. Bull.* 95, 686–700. doi:10.1130/0016-7606(1984)95<686:rraafy>2.0.co;2

Chen, J. (2013). "Response of channel offsets to dextral-slip movement of the Red River fault zone," (China: Zhejiang University). A master's degree thesis.

Chen, W. J., Li, Q., and Wang, Y. P. (1996). Miocene diachronic uplift along the Ailao mountains Red River left-lateral strike-slip shear zone. *Geol. Rev.* 5, 385–390.

Cong, D. C., and Feigl, K. L. (1999). Geodetic measurement of horizontal strain across the Red River fault near Thac Ba, Vietnam, 1963–1994. *J. Geodesy* 73, 298–310. doi:10.1007/s001900050247

Deng, Q. D., Zhang, P. Z., Ran, Y. K., Yang, X. P., Min, W., and Chu, Q. Z. (2002). The basic character of active tectonics in China. *Sci. China (Series D).* 12, 1020–1031. doi:10.3969/j.issn.1674-7240.2002.12.007

Feigl, K. L., Cong, D. C., Becker, M., To, T. D., Neumann, K., and Xuyen, N. Q. (2003). Insignificant horizontal strain across the Red River fault near Thac Ba, Vietnam from GPS measurements 1994-2000. *Geophys. Rsearch Abstr.* 5, 04707.

Gilley, L. D., Harrison, T. M., Leloup, P. H., Ryerson, F. J., Lovera, O. M., and Wang, J. H. (2003). Direct dating of left-lateral deformation along the Red River shear zone, China and Vietnam. *J. Geophys. Res.* 108 (B2), 2127. doi:10.1029/2001jb001726

Guo, S. M., Ji, F. J., Xiang, H. F., Dong, X. Q., Yan, F. H., Zhang, S. L., et al. (2001). *The Honghe active fault zone*. Beijing: Ocean Publishing House.

Guo, S. M., Xiang, H. F., Ji, F. J., and Zhang, W. X. (1996). A study on the relation between Quaternary right-lateral slip and tip extension along the Honghe fault. *Seismol. Geol.* 18, 301–309.

Hao, M., Wang, Q. L., Shen, Z. K., Cui, D. X., Ji, L. Y., Li, Y. H., et al. (2014). Present day crustal vertical movement inferred from precise leveling data in eastern margin of Tibetan Plateau. *Tectonophysics* 632, 281–292. doi:10.1016/j.tecto.2014.06.016

Harrison, T. M., Chen, W. J., Leloup, P. H., Ryerson, F. J., and Tapponnier, P. (1992). An early Miocene transition in deformation regime within the red River Fault zone, yunnan, and its significance for indo-asian tectonics. *J. Geophys. Res.* 97 (B5), 7159–7182. doi:10.1029/92jb00109

Harrison, T. M., Leloup, P. H., Ryerson, F. J., Tapponnier, P., Lacassin, R., and Chen, W. J. (1996). Diachronous initiation of transtension along the ailao Shan-Red River shear zone, yunnan and vietnam. *World Regional Geol.* 1996, 208–226.

He, X. H., Tan, S. C., Zhou, J. X., Liu, Z., Zhao, Z. F., Yang, S. Q., et al. (2020). Identifying the leucogranites in the Ailaoshan-Red River shear zone: constraints on the timing of the southeastward expansion of the Tibetan Plateau. *Geosci. Front.* 11, 765–781. doi:10.1016/j.gsf.2019.07.008

Leloup, P. H., Lacassin, R., Tapponnier, P., Scharer, U., Zhong, D. L., Liu, X. H., et al. (1995). The ailao Shan-Red River shear zone (yunnan, China), tertiary transform boundary of indo China. *Tectonophysics* 251, 3–84. doi:10.1016/0040-1951(95)00070-4

Li, X., Ran, Y. K., Chen, L. C., Wang, H., Yu, J., Zhang, Y. Q., et al. (2016). The Holocene seismic evidence on southern segment of the Red River fault zone. *Seismol. Geol.* 38, 596–604. doi:10.3969/j.issn.0253-4967.2016.03.007

McCalpin, J. P. (2009). *Paleoseismology*. Second Edition. USA: Academic Press.

Ran, Y. K., and Deng, Q. D. (1999). History, present situation and development trend of paleoseismology. *Sci. Bull.* 44, 12–20. doi:10.3321/j.issn:0023-074X.1999.01.003

Ran, Y. K., Wang, H., Li, Y. B., and Chen, L. C. (2012). Key techniques and several cases analysis in paleoseismic studies in mainland China (1): trenching sites, Layouts and Paleoseismic indicators on active strike-slip faults. *Seismol. Geol.* 34, 197–210. doi:10.3969/j.issn.0253-4967.2012.02.001

Ran, Y. K., You, H. C., Wang, J. B., Zhang, W. X., and Li, R. C. (1988). The earthquake faults of the late Quaternary on eastern piedmont of Cangshan mountain and the ages of paleoearthquakes occurring in Dali city,Yunnan Province. *Seismol. Geol.* 10 (2).

Reimer, P., Austin, W., Bard, E., Bayliss, A., Blackwell, P., Bronk Ramsey, C., et al. (2020). The IntCal20 Northern Hemisphere radiocarbon age calibration curve (0–55 cal kBP). *Radiocarbon* 62, 725–757. doi:10.1017/rdc.2020.41

Replumaz, A., Lacassin, R., Tapponnier, P., and Leloup, P. H. (2001). Large river offsets and Plio-Quaternary dextral slip rate on the Red River fault (Yunnan, China). *J. Geophys. Res.* 106 (B1), 819–836. doi:10.1029/2000jb900135

Schoenbohm, L. M., Burchfiel, B. C., Chen, L. Z., and Yin, J. Y. (2005). Exhumation of the Ailao Shan shear zone recorded by Cenozoic sedimentary rocks, Yunnan Province, China. *Tectonics* 24 (TC6015). doi:10.1029/2005TC001803

Schoenbohm, L. M., Burchfiel, B. C., Chen, L. Z., and Yin, J. Y. (2006). Miocene to present activity along the Red River fault, China, in the context of continental extrusion, upper-crustal rotation, and lower-crustal flow. *Geol. Soc. Am. Bull.* 118, 672–688. doi:10.1130/b25816.1

Searle, M. P., Yeh, M. W., Lin, T. H., and Chung, S. L. (2010). Structural constraints on the timing of left-lateral shear along the Red River shear zone in the ailao Shan and diancang Shan ranges, yunnan, SW China. *Geosphere* 6, 316–338. doi:10.1130/ges00580.1

Shen, Z. K., Lü, J. N., Wang, M., and Bürgmann, R. (2005). Contemporary crustal deformation around the southeast borderland of the Tibetan Plateau. *J. Geophys. Res.* 110, B11409. doi:10.1029/2004jb003421

Shi, X. H., Sieh, K., Weldon, R., Zhu, C. N., Han, Y., Yang, J. W., et al. (2018). Slip rate and rare large prehistoric earthquakes of the Red River fault, southwestern China. *Geochem. Geophys. Geosystems* 19, 2014–2031. doi:10.1029/2017gc007420

Tapponnier, P., Lacassin, R., Leloup, P. H., Scharer, U., Zhong, D. L., Wu, H. W., et al. (1990). The ailao Shan/Red River metamorphic belt: tertiary left-lateral shear between Indochina and South China. *Nature* 343, 431–437. doi:10.1038/343431a0

Tapponnier, P., and Molnar, P. (1976). Slip-line field theory and large scale continental tectonics. *Nature* 264, 319–324. doi:10.1038/264319a0

Tapponnier, P., Xu, Z. Q., Roger, F., Meyer, B., Arnaud, N., Wittlinger, G., et al. (2001). Oblique stepwise rise and growth of the Tibet plateau. *Science* 294, 1671–1677. doi:10.1126/science.105978

To, T. D., Yem, N. T., Cong, D. C., Hai, V. Q., Zuchiewicz, W., Cuong, N. Q., et al. (2013). Recent crustal movements of northern Vietnam from GPS data. *J. Geodyn.* 69, 5–10. doi:10.1016/j.jog.2012.02.009

Trieu, C. D. (2003). Deep structure, recent dynamics and seismic activity in Red River Fault zone in Vietnam. *J. Geodesy Geodyn.* 23, 93–102. doi:10.14075/j.jgg.2003.01.023

Wan, J. L., Li, Q., and Chen, W. J. (1997). Fission track evidence of diachronic uplift along the Ailaoshan Red River Left-lateral Strike-slip shear zone. *Seismol. Geol.* 19 (1), 87–90.

Wang, H., Liu, M., Cao, J. L., Shen, X. H., and Zhang, G. M. (2011). Slip rates and seismic moment deficits on major active faults in mainland China. *J. Geophys. Res.* 116, B02405. doi:10.1029/2010jb007821

Wang, M., and Shen, Z. K. (2020). Present-Day crustal deformation of continental China derived from GPS and its tectonic implications. *J. Geophys. Res.* 125, e2019JB018774. doi:10.1029/2019jb018774

Wang, P. L., Lo, C. H., Lee, T. Y., Chung, S. L., Lan, C. Y., and Yem, N. T. (1998). Thermochronological evidence for the movement of the Ailao Shan–Red River shear zone: a perspective from Vietnam. *Geology* 26, 887–890. doi:10.1130/0091-7613(1998)026<0887:teftmo>2.3.co;2

Wang, Y. Z., Wang, E. N., Shen, Z. K., Wang, M., Gan, W. J., Qiao, X. J., et al. (2008). GPS-constrained inversion of present-day slip rates along major faults of the Sichuan-Yunnan region, China. *Sci. China Ser. D Earth Sci.* 51, 1267–1283. doi:10.1007/s11430-008-0106-4

Xiang, H. F., Guo, S. M., Zhang, W. X., Han, Z. J., Zhang, B. L., Wan, J. L., et al. (2007). Quantitative study on the large scale dextral strike-slip offset in the southern segment of the Red River fault since Miocene. *Seismol. Geol.* 29, 52–68. doi:10.3969/j.issn.0253-4967.2007.01.003

Xiang, H. F., Han, Z. J., Guo, S. M., Zhang, W. X., and Chen, L. C. (2004). Large-scale dextral strike-slip movement and asociated tectonic deformation along the Red River fault zone. *Seismol. Geol.* 26, 597–610. doi:10.3969/j.issn.0253-4967.2004.04.006

Xuan, S. B., Shen, C. Y., Shen, W. B., Wang, J. P., and Li, J. G. (2018). Crustal structure of the southeastern Tibetan Plateau from gravity data: new evidence for clockwise movement of the Chuan–Dian rhombic block. *J. Asian Earth Sci.* 159, 98–108. doi:10.1016/j.jseaes.2018.03.018

Yin, F. L., Jiang, C. S., Han, L. B., Zhang, H., and Zhang, B. (2018). Seismic hazard assessment for the Red River fault: insight from Coulomb stress evolution. *Chin. J. Geophys.* 61, 183–198. doi:10.6038/cjg2018L0369

Yu, N., Unsworth, M., Wang, X. B., Li, D. W., Wang, E. C., Li, R. H., et al. (2020). New insights into crustal and mantle flow beneath the red River Fault zone and adjacent areas on the southern margin of the Tibetan plateau revealed by a 3-D magnetotelluric study. *J. Geophys. Res.* 125, e2020JB019396. doi:10.1029/2020jb019396

Zhang, B. L., Liu, R. X., Xiang, H. F., Wan, J. L., and Huang, X. N. (2009). FT dating of fault rocks in the central southern section of the Red River fault zone and its geological implications. *Seismol. Geol.* 31, 44–56. doi:10.3969/j.issn.0253-4967.2009.01.005

Zhang, J. G., Xie, Y. Q., Jin, M. P., Li, X., Ye, J. Q., Mao, X., et al. (2009). *Red River fault activity in China and vietnam. Kunming*. Kunming, Yunnan: Yunnan Science and Technology Publishing House.

Zhang, P. Z., Shen, Z. K., Wang, M., and Gan, W. J. (2004). Kinematics of present-day tectonic deformation of the Tibetan plateau and its vicnities. *Seismol. Geol.* 26, 367–377. doi:10.3969/j.issn.0253-4967.2004.03.002

Zhang, P. Z., Wang, Q., and Ma, Z. J. (2002). GPS velocity field and active crustal blocks of contemporary tectonic deformation in continental China. *Earth Sci. Front.* 9, 430–441. doi:10.3321/j.issn:1005-2321.2002.02.022

Zhao, J., Jiang, Z. S., Wu, Y. Q., Liu, X. X., and Wei, W. X. (2012). Characteristics of block strain and fault movement in the Sichuan-Yunnan region before and after Wenchuan earthquake. *Geodesy Geodyn.* 3, 27–33. doi:10.3724/sp.j.1246.2012.00027.1

Zheng, G., Wang, H., Wright, T. J., Lou, Y. D., Zhang, R., Zhang, W. X., et al. (2017). Crustal deformation in the India-eurasia collision zone from 25 Years of GPS measurements. *J. Geophys. Res.* 122, 9290–9312. doi:10.1002/2017jb014465

Zuchiewicz, W., and Cuong, N. Q. (2009). Quaternary tectonics of the red River Fault zone in vietnam-A morphotectonic approach. *Geologia* 35, 367–374.